A PDE Approach for Measuring Tissue Thickness

Anthony Yezzi* and Jerry L. Prince†
*School of Electrical and Computer Engineering
Georgia Institute of Technology, Atlanta, GA 30332-2050
†Department of Electrical and Computer Engineering
John Hopkins University, Baltimore, MD 21218

Abstract

We outline an Eulerian framework for computing the thickness of tissues between two simply connected boundaries. Thickness is defined as the length of trajectories which follow a smooth vector field constructed in the region between the boundaries. A pair of partial differential equations (PDE's) are then solved and combined to yield length without requiring the explicit construction of the trajectories. An efficient, stable, and computationally fast solution to these PDE's is found by careful selection of finite differences according to an upwinding condition. The behavior and performance of our method is demonstrated on two simulations and two magnetic resonance imaging data sets in two and three dimensions. These experiments reveal very good performance and show strong potential for application in tissue thickness visualization and quantification.

1. Introduction

Measuring the thickness of anatomical objects is an important objective in medical image analysis for several reasons. For one, the thickness of a particular structure might provide an indication of its functional performance. For example, myocardial thickening during systole is an important indicator of heathly cardiac function [1]. Thickness can also provide an indication of disease. For example, thinning of the gray matter in the brain cortex is thought to be associated with Alzheimer's disease and other neurodegenerative disorders [2]. Thickness might also prove to be the basis for image segmentation. For example, it is well known that the anterior and posterior banks of the central sulcus in the human brain cortex can be distinguished by a difference in thickness alone [3]. Finally, thickness can be used as a basis for efficient characterization of anatomical shape when coupled with a central axis representation [4].

In this paper, we present a method for computing the thickness between two surfaces (or curves) that do not have point correspondences defined between them. The method we describe is based on the definition of thickness as the length of trajectores (curved, in general) from one surface to the other. While conceptually analogous to the thickness definition used in [5], our definition is more general and our computational approach is fast and stable. After presenting our algorithm, we give two simulations and two additional examples from cardiac and brain images demonstrating its performance.

2. Thickness Definition

There have been many definitions of anatomical thickness in the literature. Left ventricular myocardial thickness is most often defined within a cross-sectional image, and is assumed to be the distance[1] between the endocardium and epicardium along a line passing through the long-axis of the ventricle [6] (thought of as the origin), as shown in Fig. 1(a). This definition does not capture the three-dimensional aspect of the heart wall, requires that the positions of the endocardium and epicardium are radial functions, and depends on the (arbitrarily defined) location of the long-axis. Most often, the papillary muscles are not included in the segmentation of the endocardium in order to make sure that the endocardium is a radial function. With the increasing resolution of magnetic resonance (MR) images, a more precise, three-dimensional, definition of thickness that is not susceptible to user variation is needed.

Brain cortex thickness has been defined in several ways. Coupled-surface methods, such as that in [7] and [8] typically define thickness as the distance between point pairs uniquely associated between the two surfaces. One problem with this approach is that the thickness measures will be artifically high if the two surfaces are displaced relative to one another, as shown in Fig. 1(b) (solid lines). This problem is addressed in [2], where the thickness is defined as the average of the two distances to the closest points on the opposing surfaces for each of the two paired points, as shown in Fig. 1(b) (dotted lines). This definition, however, loses the idea of unique point association between the two surfaces, and can also yield thickness measures that are too small, as demonstrated in Fig. 1(c).

[1]The word *distance* means *Euclidean distance* unless otherwise stated.

0-7695-1272-0/01 $10.00 © 2001 IEEE

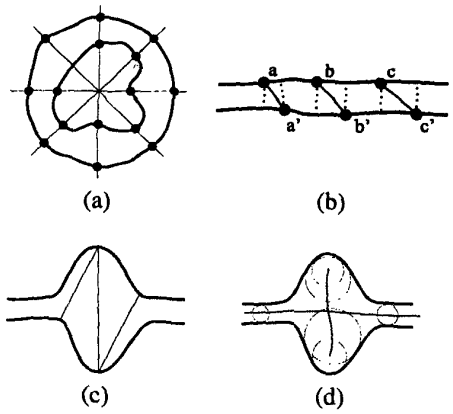

Figure 1: Problems related to thickness definitions.

Uncoupled surface thickness measures do not have *a priori* point associations between the two surfaces. A simple measure of thickness in this case is to simply measure the distance from each point on a given surface to the closest point on the opposing surface [9]. The most obvious flaw with this definition is the lack of symmetry — the thickness is not the same when the surfaces are interchanged. Also, the thickness can be dramatically underestimated using this approach when there is a pronounced bulge in the opposing surface. Both of these problems are demonstrated in Fig. 1(c). It is possible to create point associations between the surfaces by shape matching [10, 11]. However, the standard definitions of thickness for coupled surfaces would now apply, and these suffer from the flaws outlined above.

Another class of methods define thickness relative to a central axis or skeleton [4]. Generally, there is no point association between the central axis and the two surfaces, and thickness is typically treated as the diameter of the largest enclosed sphere centered at a given point on the central axis. The problem with this definition is that the skeleton will have to take on an arbitrary topology in order to properly describe highly-convoluted objects. An abrupt change in thickness, for example, might require that the skeleton grow a branch in order to completely define the geometry of the two surfaces, as shown in Fig. 1(d). If on the other hand, the topology of the central axis is restricted — to that of a simple sheet, for example — then the resulting thickness measurement often underestimates the actual thickness when either of the two surfaces is bumpy. Other definitions, such as the distance *orthogonal* to a central axis, are fraught with difficulties, as is easily demonstrated by experimenting with simple examples.

Jones et al. [5] proposed a new measure of cortical thickness based on curved lines connecting the two bounding surfaces. They proposed setting the potential of one surface to zero, setting the potential of the other surface to one, and solving Laplace's equation for the potential between the two surfaces (as in an electric field). The lengths of the lines of flow between the two surfaces then defines the thickness. These lines have desirable properties: they are orthogonal to each surface, they do not intersect, and they are nominally parallel. In this paper, we generalize this framework and specifically address the computation of trajectory lengths, which Jones et al. implemented by explicit tracking of the lines in a Lagrangian framework. Here, we present an Eulerian framework that leads to a computationally stable and fast algorithm.

3. General Approach

In this section, we outline a mathematical approach for measuring the thickness of segmented tissues using a pair of linear partial differential equations. Specifically, we show how a simple linear PDE can be used to compute trajectory lengths at all points using only the vector field of unit tangents. The unit tangent field can be constructed by any (reasonable) process, including by computing the normalized gradient of a harmonic function as in Jones et al. [5]. Solution of the identified PDE's eliminates the need to explicitly construct and measure any individual trajectory.

We assume that the tissue to be measured occupies a spatial region R with exactly two simply connected boundaries $\partial_0 R$ and $\partial_1 R$, which we call the inner and outer boundaries, respectively. We define thickness at any point $\mathbf{x} \in R$ as the total arclength of a unique curve, passing through $\mathbf{x}$, which originates on $\partial_0 R$ and terminates on $\partial_1 R$. Uniquness is necessary in this definition in order to avoid ambiguity; it implies that we can construct a family of nonintersecting curves connecting the boundaries in a bijective fashion. These curves, which we refer to as *correspondence trajectories*, also associate unique points on the boundaries to each point $\mathbf{x}$ in R.

Correspondence trajectories cannot, in general, be established via "closest point" relations between the two boundaries (see Section 2). However, there are an infinite number of vector fields defined on R whose streamlines satisfy the uniqueness requirements. Additional desirable properties narrow the list of candidates. For example, correspondence trajectories should approach a boundary from a normal direction, they should proceed as directly as possible from one boundary to the other, and their speed should never go to zero.

It is convenient to construct a unit vector field which coincides with the tangent vectors of the correspondence trajectories. There are many possible choices, and the framework we will outline applies equally well to any particular choice. One possible choice is a normalized gradient vec-

tor flow field [12], where the boundaries play the role of edge maps. Another choice is the normalized gradient of the unique harmonic function u over R that interpolates between 0 along $\partial_0 R$ and 1 along $\partial_1 R$. This is the function used by Jones et al. [5], and is what we also use in the experiments presented in this paper. We obtain the harmonic function u and the corresponding tangent field $\vec{T}$ by solving the Laplace equation over R:

$$\Delta u = 0 \tag{1}$$

$$u(\partial_0 R) = 0 \quad \text{and} \quad u(\partial_1 R) = 1 \tag{2}$$

$$\vec{T} = \frac{\nabla u}{\|\nabla u\|} \tag{3}$$

Typically the tissue region R to be measured is given as a set of pixels or voxels on a rectangular grid. Thickness is defined at each point in R as the length of its correspondence trajectory. We now show that it is not necessary to explicitly construct the trajectories — e.g., by tracing the flow of particles — in order to calculate these lengths. The key is to devise an Eulerian framework that utilizes the fixed rectangular grid and to exploit the unit tangent field in a particular differential structure.

Let us assume that we are given a unit vector field $\vec{T}(\mathbf{x})$ defined on R such that the orientations of these tangents follow correspondence trajectories directed from the inner boundary $\partial_0 R$ to the outer boundary $\partial_1 R$. It follows that $-\vec{T}(\mathbf{x})$ follows the same correspondence trajectories but is directed from $\partial_1 R$ to $\partial_0 R$. We define two length functions, L_0 and L_1, where $L_0(\mathbf{x})$ gives the arclength of the correspondence trajectory between $\partial_0 R$ and $\mathbf{x}$, and $L_1(\mathbf{x})$ gives the arclength of the trajectory between $\partial_1 R$ and $\mathbf{x}$.

It follows from elementary differential geometry that the length functions L_0 and L_1 must satisfy the following first-order linear partial differential equations:

$$\nabla L_0 \cdot \vec{T} = 1 \quad \text{with} \quad L_0(\partial_0 R) = 0 \tag{4}$$

$$-\nabla L_1 \cdot \vec{T} = 1 \quad \text{with} \quad L_1(\partial_1 R) = 0 \tag{5}$$

We describe an efficient numerical scheme to simultaneously solve these PDE's in Section 4. Then, since the length functions L_0 and L_1 measure the arclengths starting from opposite endpoints of each correspondence trajectory, the total arclength of the trajectory through any point $\mathbf{x}$ is obtained by adding $L_0(\mathbf{x})$ and $L_1(\mathbf{x})$:

$$\text{Thickness} = L_0 + L_1. \tag{6}$$

In this fashion, thickness is computed at every point in R without ever explicitly constructing a correspondence trajectory. We now proceed to describe the numerical solution of (4) and (5).

4. Numerical Implementation

Since there are many standard numerical methods for solving (1) in order to obtain $\vec{T}$ via (3), and since there are many other natural ways to choose the tangent field without using the Laplace equation, we will not go into detail about the numerical computation of $\vec{T}$. Instead, we focus our attention here on the development of a numerical scheme for solving the PDE's (4) and (5) to obtain the length functions L_0 and L_1 assuming we are given the tangent field $\vec{T}$. We note that the characteristics of these PDE's are exactly the correspondence trajectories. Therefore, because the correspondence trajectories never intersect, we do not need to worry about shocks, in contrast to many first-order boundary value problems (such as the Eikonal equation, which would yield "closest point" correspondences). Because of this, we do not need to be concerned with entropy conditions in the numerical schemes to solve these PDE's, although appropriate upwinding will be crucial.

Here, we will consider only the case of a 3D rectangular grid with spacing h_x, h_y, and h_z between neighboring grid points (voxels) in the x, y, and z directions respectively. The 2D case is simply a special case of the 3D case. The notation $T_x[i,j,k]$, $T_y[i,j,k]$, and $T_z[i,j,k]$ denotes the components of $\vec{T}$ at the grid point (i,j,k), and backward and forward differences are given by the following standard notation [14, 15, 16]

$$D_x^- L = \frac{L[i,j,k] - L[i-1,j,k]}{h_x}, \quad D_x^+ L = \frac{L[i+1,j,k] - L[i,j,k]}{h_x}$$

$$D_y^- L = \frac{L[i,j,k] - L[i,j-1,k]}{h_y}, \quad D_y^+ L = \frac{L[i,j+1,k] - L[i,j,k]}{h_y}$$

$$D_z^- L = \frac{L[i,j,k] - L[i,j,k-1]}{h_z}, \quad D_z^+ L = \frac{L[i,j,k+1] - L[i,j,k]}{h_z}$$

Upwind differencing. We start by considering various combinations of the above first-order differences to approximate ∇L_0 in (4), yielding various linear expressions for $L_0[i,j,k]$ in terms of three of its six neighbors $L_0[i\pm1,j,k]$, $L_0[i,j\pm1,k]$, and $L_0[i,j,k\pm1]$.

$$\begin{aligned} 1 = {} & T_x[i,j,k]\left(D_x^- L_0[i,j,k] \text{ or } D_x^+ L_0[i,j,k]\right) \\ & + T_y[i,j,k]\left(D_y^- L_0[i,j,k] \text{ or } D_y^+ L_0[i,j,k]\right) \\ & + T_z[i,j,k]\left(D_z^- L_0[i,j,k] \text{ or } D_z^+ L_0[i,j,k]\right) \end{aligned} \tag{7}$$

Since (4) is a first order PDE with known boundary values, its solution may be constructed by integration along characteristic curves starting from the known boundary. By design, the characteristics of (4) are precisely the correspondence trajectories, and therefore the tangent vector $\vec{T}[i,j,k]$ tells us which direction the characteristic through the grid point $[i,j,k]$ is flowing.

We do not need to worry about shocks and entropy conditions [13, 14, 15, 16] since the characteristics of the linear PDE's (4)–(5) never intersect. On the other hand, information does flow in the forward direction (downwind) along the characteristics, so it is important to choose our differencing scheme (i.e. D_x^- vs. D_x^+, ...) so that the value of $L_0[i,j,k]$ only depends upon values of L_0 in the backward direction (upwind) along the characteristic passing through the grid point [i,j,k]. This direction is given by $-\vec{T}[i,j,k]$. Therefore, upwinding dictates the following choice for (7).

$$\begin{aligned} 1 = {} & T_x[i,j,k] \begin{cases} D_x^- L_0[i,j,k], & -T_x[i,j,k] < 0 \\ D_x^+ L_0[i,j,k], & \text{otherwise} \end{cases} \\ & + T_y[i,j,k] \begin{cases} D_y^- L_0[i,j,k], & -T_y[i,j,k] < 0 \\ D_y^+ L_0[i,j,k], & \text{otherwise} \end{cases} \\ & + T_z[i,j,k] \begin{cases} D_z^- L_0[i,j,k], & -T_z[i,j,k] < 0 \\ D_z^+ L_0[i,j,k], & \text{otherwise} \end{cases} \end{aligned} \tag{8}$$

Solving (8) for $L_0[i,j,k]$ and an analogous upwind scheme for $L_1[i,j,k]$ (noting that the upwind direction for L_1 is given by $\vec{T}$ rather than $-\vec{T}$) yields the following finite difference approximations (where, for simplicity, we assume that $h_x = h_y = h_z = 1$):

$$L_0[i,j,k] = \frac{1 + |T_x| L_0[i \mp 1, j, k] + |T_y| L_0[i, j \mp 1, k] + |T_z| L_0[i, j, k \mp 1]}{|T_x| + |T_y| + |T_z|} \tag{9}$$

$$L_1[i,j,k] = \frac{1 + |T_x| L_1[i \pm 1, j, k] + |T_y| L_1[i, j \pm 1, k] + |T_z| L_1[i, j, k \pm 1]}{|T_x| + |T_y| + |T_z|} \tag{10}$$

$$i \pm 1 = \begin{cases} i+1, & T_x > 0 \\ i-1, & T_x < 0 \end{cases} \quad j \pm 1 = \begin{cases} j+1, & T_y > 0 \\ j-1, & T_y < 0 \end{cases} \quad k \pm 1 = \begin{cases} k+1, & T_z > 0 \\ k-1, & T_z < 0 \end{cases}$$

Iterative procedure. We now use (9) and (10) in the following iterative procedure to solve for the correspondence trajectory lengths L_0 and L_1 (given the tangent field $\vec{T}$):

1. Set $L_0 = L_1 = 0$ at all grid points.
   (Values outside R will serve as boundary conditions.)
2. Use (9)–(10) to update L_0 and L_1 at points inside R.
3. Repeat step 2 until the values L_0 and L_1 converge.

If the values of L_0 and L_1 are updated in place so that new values at each point are used when updating the values of the next point (a Gauss-Siedel type procedure), then convergence will occur very quickly, assuming that points in R are visited in a reasonable order. In particular, if we visit the points in the order that they are reached by the characteristic curves (the correspondence trajectories) as they flow from the known boundary, then only one full pass through the grid points in R is required for each length function. This would require an algorithm similar to "Fast Marching" (used to solve the Eikonal equation, see [16, 17]) in which the values of L_0 and L_1 are computed outward from the known boundaries along the characteristics. Note that the "marching order" would be different for L_0 and L_1.

A simpler scheme that still converges very quickly (but avoids the book-keeping required for the optimal scheme) is to cyclically alternate the order that the grid points in R are updated during each iteration using orderings related to the rectangular grid structure. For example, in the first iteration, grid points $[i,j,k]$ could be visited in order of increasing i, increasing j, and increasing k; while in the next iteration they could be visited in order of decreasing i, increasing j, and increasing k, and so on (8 different combinations for a 3D grid or 4 combinations for a 2D grid). If the correspondence trajectories are not highly convoluted, there will be large sub-regions of R during each iteration, where the characteristics run approximately along the current i, j, and k directions, and thus the optimal marching procedure will be closely approximated within these sub-regions. This cyclical Gauss-Siedel procedure converges in fewer than 10 iterations for all the experiments in Section 5.

Finally, note that although we initialize L_0 and L_1 to be 0 outside *both boundaries* (even though each length function should have a boundary condition of 0 along only one of the two boundaries), the update equations (9) and (10) are designed to look in opposite directions. Thus, one scheme will affected by the zero boundary condition only along the inner boundary, while the outher will be affected only along the outer boundary. Therefore, it is possible to update L_0 and L_1 simultaneously (as indicated in step 2), using zero boundary conditions (from step 1) on both sides, which greatly simplifies the procedure.

5. Experimental Results

In this section, we demonstrate our approach for computing thickness on both synthetic test regions with known values and segmented tissue regions in real images. The first three experiments are on 2D regions (which can be fully visualized), while the last experiment is in 3D.

To test our algorithm, we constructed an annulus between two concentric circles of radii 80 and 160 (all units in pixels), as shown in Fig. 2(a). It is clear that the thickness of this region should be 80 everywhere. Fig. 2(b) shows the harmonic function u which interpolates between 0 and 1 along the inner and outer boundaries, and the normalized gradient of u, which comprises the tangent field $\vec{T}$, is shown in Fig. 2(c). The trajectory lengths L_0 and L_1 were computed using (9) and (10), and their sum, the thickness, is shown in Fig. 2(d). The experimental values ranged between 79.84 and 80.30.

As another test, we constructed an annulus between a cir-

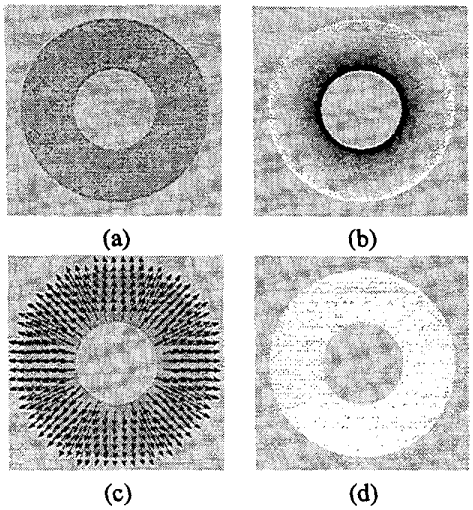

Figure 2: (a) Annular region and its (b) harmonic interpolant. (c) The tangent field and (d) the computed thickness.

cle of radius 40 (all units in pixels) and an ellipse with minor and major radii of 80 and 160, as shown in Fig. 3(a). This time, the computed thickness values ranged from (approximately) 40 to 120 as we move from points near the minor axis towards points near the major axis. Note that the correspondence trajectories are straight lines only along these two axes. Away from these axes, the trajectories are slightly curved in order to remain perpendicular to both boundaries and to avoid intersection. The computed trajectories can be visualized in Fig. 4, which gives some level sets of the computed thickness function shown in Fig. 3(d).

Next, we applied our method to a segmentation of the myocardium obtained from a short-axis MR image of the heart, both of which are shown in Fig. 5(a). A subsample of the tangent vectors computed from solution of Laplace's equation are shown in Fig. 5(b). Evidence of the need to form curved correspondence trajectoried is apparent inside the papillary muscle appearing at about 3 o'clock on the inside boundary. The calculated thickness is shown in Fig. 5(c), which shows brighter regions where one sees thicker myocardium. An isocontour plot showing some of the correspondence trajectories is shown in Fig. 5(d). These show the curved trajectories over which thickness is (implicitly) computed.

Finally, we applied our method to a 3D segmentation of the cortex obtained from MR images of the brain. One of the original coronal cross-sections is shown in Fig. 6(a) and the inner and outer segmentation results are shown in Figs 6(b) and 6(c), respectively. Thickness was computed in the region between these two boundaries, and the results for the cross-section shown in Fig. 6(a) are shown in Fig. 6(d). The result is brighter (meaning thicker) in regions where

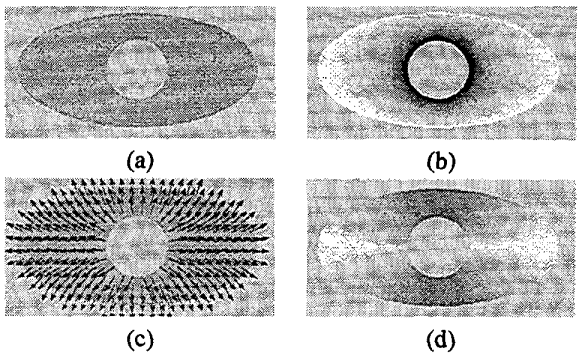

Figure 3: (a) Region between a circle and an ellipse, (b) harmonic interpolant, (c) the tangent field, and (d) the computed thickness.

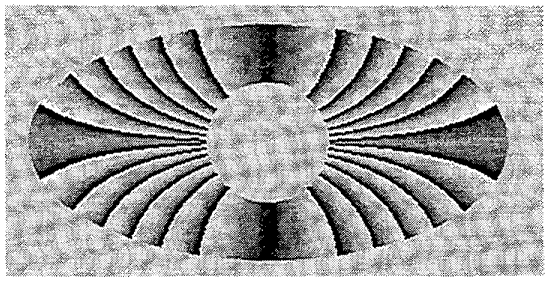

Figure 4: Level sets of thickness function.

one would expect this given the segmentation (although one has to be cautious about interpreting the thickness of a 3D object from its cross-sections). The fact that there are erroneous thickness measures occur around several sulci (inward folds of the cortex) and the hippocampus and thalamus are included reflect on the quality of the segmentation result (which was not optimized for this experiment), not the thickness computation.

6. Conclusion

We have presented a fast and accurate method for computing the thickness of segmented objects bounded by two contours or surfaces. Our method was motivated by the need to measure thickness in various tissues seen in medical images. The method uses a two-stage approach in which a unit tangent field is first constructed by appropriate means — e.g., the solution of Laplace's equation within the object — and then the thickness is computed by combining the solution of two linear, first-order PDE's. The numerical method is constructed by using appropriate upwinding conditions within an iterative finite differencing framework. In certain medical imaging applications, this algorithm might eventually be thought of as a companion to segmentation, producing thickness data carrying significant diagnostic and/or scientific value. As well, we believe that this overall two-

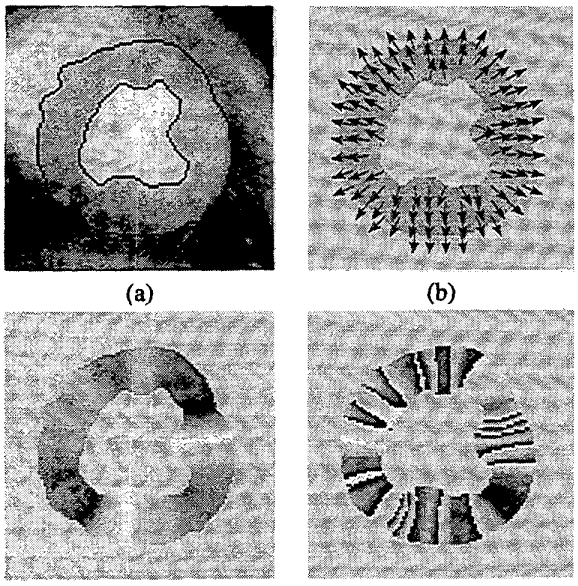

Figure 5: Myocardial thickness from a short-axis MR image.

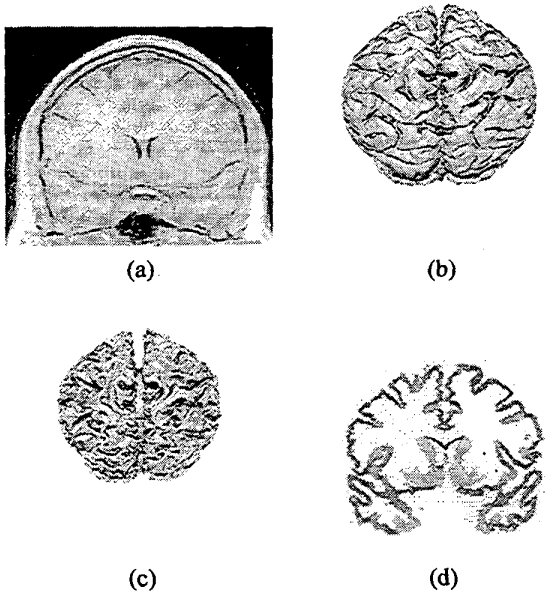

Figure 6: 3D cortical thickness calculation.

stage Eulerian PDE approach has potential for use in other applications besides medical imaging, and for other computations besides thickness.

References

[1] M. E. DeBakey and A. M. Gotto Jr. *The New Living Heart.* Adams Media Corporation, Holbrook, MA, 1997.

[2] B. Fischl and A. M. Dale. Measuring the thickness of the human cerebral cortex from magnetic resonance images. *Proc. Nat. Acad. Sci.*, 97(20):11050–11055, 2000.

[3] J. Nolte and J. B. Angevine Jr. *The Human Brain: In Photographs and Diagrams.* Mosby, St. Louis, 1995.

[4] S.M. Pizer, D. Eberly, D.S. Fritsch, and B.S. Morse. Zoom-invariant vision of figural shape: the mathematics of cores. *Comp. Vis. Imag. Under.*, 69(1):55–71, 1998.

[5] S. E. Jones, B. R. Buchbinder, and Itzhak Aharon. Three-dimensional mapping of the cortical thickness using Laplace's equation. *Hum. Brain. Mapp.*, 11:12–32, 2000.

[6] W. Grossman. Assessment of regional myocardial function. *J. Am. Coll. Cardiol.*, 7(2):327–328, 1986.

[7] D. MacDonald, N. Kabani, D. Avis, and A. C. Evans. Automated 3-d extraction of inner and outer surfaces of cerebral cortex from MRI. *NeuroImage*, 12:340–356, 2000.

[8] X. Zeng, L.H. Staib, R.T. Schultz, and J.S. Duncan. Segmentation and measurement of the cortex from 3-D MR images using coupled-surfaces propagation. *IEEE Trans. Med. Imag.*, 18(10):927–937, October 1999.

[9] M. Miller, A. Massie, J. Ratnanather, K. Botteron, and J. Csernansky. Bayesian construction of geometrically based cortical thickness metrics. *NeuroImage*, 12:676–687, 2000.

[10] J. C. McEachen II and J. S. Duncan. Shape-based tracking of left ventricular wall motion. *IEEE Trans. Med. Imag.*, 16(3):270–283, 1997.

[11] H. D. Tagare. Deformable 2-D template matching using orthogonal curves. *IEEE Transactions on Medical Imaging*, 16(1):108–117, February 1997.

[12] C. Xu and J.L. Prince. Snakes, Shapes, and Gradient Vector Flow. *IEEE Transactions on Image Processing*, 7(3): 359–369, March 1998.

[13] R. J. LeVeque, *Numerical Methods for Conservation Laws*, Birkhäuser, Boston, 1992.

[14] S. Osher, "Riemann solvers, the entropy condition, and difference approximations," *SIAM J. Numer. Anal.*, vol. 21, pp. 217–235, 1984.

[15] S. Osher and J. Sethian, "Fronts propagation with curvature dependent speed: Algorithms based on Hamilton-Jacobi formulations," *Journal of Computational Physics*, vol. 79, pp. 12–49, 1988.

[16] J. Sethian, *Level Set Methods: Evolving Interfaces in Geometry, Fluid Mechanics, Computer Vision, and Material Science*, Cambridge University Press, 1996.

[17] J. Tsitsiklis, "Efficient Algorithms for Globally Optimal Trajectories," *IEEE Trans. Aut. Control*, 40:1528-1538, 1995.